The Astrophysical Journal, 684:34–45, 2008 September 1

A COMPARISON OF WEAK-LENSING MEASUREMENTS FROM GROUND- AND SPACE-BASED FACILITIES

Mansi M. Kasliwal,[1,2] Richard Massey,[1] Richard S. Ellis,[1] Satoshi Miyazaki,[3] and Jason Rhodes[1,4]
Received 2007 October 18; accepted 2008 March 5

ABSTRACT

We assess the relative merits of weak-lensing surveys, using overlapping imaging data from the ground-based Subaru telescope and the *Hubble Space Telescope* (*HST*). Our tests complement similar studies undertaken with simulated data. From observations of 230,000 matched objects in the 2 deg^2 COSMOS field, we identify the limit at which faint galaxy shapes can be reliably measured from the ground using well-established shape-measurement techniques. Our ground-based shear catalog achieves subpercent calibration bias compared to high-resolution space-based data for galaxies brighter than $i' \simeq 24.5$ and with half-light radii larger than $1.8''$. This selection corresponds to a surface density of 15 galaxies arcmin^{-2} compared to $\sim$71 arcmin^{-2} from space. On the other hand, the survey speed of current ground-based facilities is much faster than that of *HST*, although this gain is mitigated by the increased depth of space-based imaging desirable for tomographic (3D) analyses. As an independent experiment, we also reconstruct the projected mass distribution in the COSMOS field using both data sets, and compare the derived cluster catalogs with those from X-ray observations. The ground-based catalog achieves a reasonable degree of completeness, with minimal contamination and no detected bias, for massive clusters at redshifts $0.2 < z < 0.5$. The space-based data provide improved precision and a greater sensitivity to clusters of lower mass or at higher redshift.

Subject headings: atmospheric effects — cosmology: observations — gravitational lensing — instrumentation: detectors

Online material: color figures

1. INTRODUCTION

Dark matter dominates the gravitational component of the cosmic energy density and thus provides the framework for structure formation in the universe. However, by its nature the distribution and cosmic growth are challenging to observe. The most promising probe is weak gravitational lensing: analysis of the distorted shapes of ordinary galaxies behind foreground mass concentrations. Several numerical techniques are now available to recover the projected mass distribution from these distortions, and tests on simulated data sets have been done to verify their precision (Heymans et al. 2005a; Massey et al. 2007d). There is great optimism in the weak-lensing community that such methods will enable the tomographic mapping of dark matter structures in both time and space. This will also provide a robust statistical measure of the nature of dark energy over redshifts $0 < z < 1$ (Mellier 1999; Refregier 2003).

Observational progress has been particularly dramatic. The first detections of statistical "cosmic shear" were only published in 2000 (Bacon et al. 2000; Kaiser et al. 2000; Wittman et al. 2000; van Waerbeke et al. 2000). In the subsequent 8 years, weak-lensing surveys have measured the dark matter power spectrum (Brown et al. 2003; Heymans et al. 2005b; Hoekstra et al. 2006; Semboloni et al. 2006), traced the evolution of structure (Bacon et al. 2005; Kitching et al. 2007; Massey et al. 2007b), enabled the construction of lensing-selected cluster catalogs (Miyazaki et al. 2002a, 2007; Wittman et al. 2006; Schirmer et al. 2007), and nonparametrically reconstructed the total mass distribution both in clusters (Kneib et al. 2003; Clowe et al. 2006b; Jee et al. 2007a) and on larger scales (Massey et al. 2007c). As a result, weak lensing has been identified as the most promising route to understanding the nature of dark energy by the ESA-ESO Working Group on Fundamental Cosmology,[5] the joint NSF-NASA-DOE Astronomy and Astrophysics Advisory Committee,[6] and the NSF-DOE High Energy Physics Advisory Panel Dark Energy Task Force.[7]

The primary signal of any weak-lensing analysis is the statistically coherent distortion of background galaxies along adjacent lines of sight. The main sources of statistical noise are the finite density of galaxies that can be sufficiently well detected and resolved for accurate shape measurement, plus their intrinsic morphologies. The density of resolved galaxies also governs the angular resolution and fidelity of a reconstructed mass map which, in turn, determines the limiting halo mass that can be detected. On the other hand, statistical analyses of the dark matter power spectrum are less concerned with individual halos but require panoramic fields to counter the effects of cosmic (sample) variance. Minimizing statistical errors in such an analysis, within a finite survey lifetime, requires an optimal balance between area and depth.

A key debate in the development of future weak-lensing experiments concerns the relative merits of ground- versus space-based platforms. Ambitious surveys are now being planned with dedicated, ground-based facilities (e.g., VST-KIDS, DES, Pan-STARRS, and LSST).[8] These are driven by technological progress, including panoramic cameras with small optical distortions,

[1] California Institute of Technology, MS 105-24, Pasadena, CA 91125.
[2] George Ellory Hale Fellow of Moore Foundation.
[3] National Astronomical Observatory of Japan, Mitaka, Tokyo 181-8588, Japan.
[4] Jet Propulsion Laboratory, California Institute of Technology, MS 169-506, Pasadena, CA 91125.

[5] See http://www.stecf.org/coordination/esa_eso/cosmology.php.
[6] See http://www.nsf.gov/mps/ast/aaac.jsp.
[7] See http://www.nsf.gov/mps/ast/detf.jsp.
[8] See http://www.astro-wise.org/projects/KIDS/, https://www.darkenergysurvey.org/, http://pan-starrs.ifa.hawaii.edu/public/, and http://www.lsst.org/lsst_home.shtml, respectively.

highly sensitive imaging detectors, and (in the case of Pan-STARRS) on-chip active correction to reduce the width of the point-spread function (PSF). Future surveys spanning significant fractions of the celestial sphere are envisaged, promising tight constraints on the cosmological parameters.

However, measurements with current ground-based facilities are limited by the size and temporal variations of the PSF. There is concern in many quarters that wide-field facilities operating in space (e.g., *JDEM*)[9] will ultimately be required to achieve the precision required (particularly) to distinguish between various models of dark energy. Space-based facilities may be more costly but will likely offer increased depth, better photometric performance, and a stable PSF. The key issue in gauging their merits is not statistical error, but the extent to which potential biases in ground-based data may act as a "systematic floor" to prevent complete exploitation.

Some quantitative comparisons can be obtained by contrasting simulations of ground- and space-based images (Wittman et al. 2005; Lampton et al. 2006), and from the Shear Testing Program (STEP; Heymans et al. 2005a; Massey et al. 2007d). The STEP approach is to examine various methods using idealized data; our complementary approach is to examine realistic *data* using well-established methods. For example, STEP modeled neither the instability nor vagaries of a real PSF—which may, ultimately, be the limiting problem for ground-based data. It is often argued that future facilities will be carefully designed to mitigate any limitations of current observational facilities. While technological progress can no doubt be expected both on the ground and in space, bringing observations toward those modeled by STEP, we believe many lessons can be learned from extant data and hardware with proven engineering pedigree. The actual limitations of a future experiment will, realistically, be governed by factors revealed by both approaches. However, it is ground-based observations that are currently farthest from ideal. Addressing the causes of systematic effects in space-based lensing experiments will be a purely engineering task aimed at hardware improvements and thermal stability. Future ground-based experiments will not only address engineering issues but will continue to be plagued by the uncontrollable vagaries of the atmosphere.

In this paper we present the first direct and detailed comparison of weak-lensing analysis *for the same sky field* using ground- and space-based data. Deep, panoramic imaging has been obtained for the 1.64 deg^2 COSMOS field (Scoville et al. 2007a) by both the Advanced Camera for Surveys (ACS) on board the *Hubble Space Telescope* (*HST*; Scoville et al. 2007b) and the Suprime-Cam imager at the prime focus of the Subaru 8.2 m telescope (Taniguchi et al. 2007). In both cases, the entire field was covered by mosaicking many independent exposures. The Suprime-Cam instrument was constructed with weak-lensing analysis particularly in mind, and currently provides the best image performance available from any ground-based telescope, in terms of optical distortions over a large field. A comparison of these data sets should therefore provide a realistic and valuable assessment of the relative performance of state-of-the-art imagers on the ground and in space.

The paper is organized as follows. In § 2 we briefly review the relevant theory. In § 3 we describe the two data sets, data reduction pipelines, and weak-lensing analyses. We then present the results. In § 4 we compare shear measures on a galaxy-by-galaxy basis to determine the optimum depth at which the ground-based data match the performance of the (deeper) space-based data. This permits us to determine the relative survey speeds of Subaru and *HST* for high-precision cosmic shear experiments. In § 5 we construct maps of the mass distribution, treating the Subaru and *HST* maps as independent probes of the same field, and contrast these against X-ray data. This permits us to evaluate the completeness and reliability of a lensing-selected halo catalog, and evaluate the precision of their inferred masses as a function of redshift. In § 6 we summarize our results and discuss their wider implications.

[9] See http://universe.nasa.gov/program/probes/jdem.html .

2. REVIEW OF WEAK-LENSING THEORY

Gravitational lensing by foreground mass structures distorts an image plane of distant galaxies $I(\boldsymbol{x})$ via a coordinate transformation

$$\mathcal{A}_{ij} = \delta_{ij} + \frac{\partial(\delta x_i)}{\partial x_j} = \begin{pmatrix} 1-\kappa-\gamma_1 & \gamma_2 \\ \gamma_2 & 1-\kappa+\gamma_1 \end{pmatrix}, \quad (1)$$

where $\delta x_i(\boldsymbol{x})$ is the deflection angle of the light rays. The *convergence*,

$$\kappa(\boldsymbol{x}) = \frac{4\pi G}{2c^2}\int g(z)\rho(\boldsymbol{x},z)\,dz, \quad (2)$$

describes overall dilations and contractions. It is proportional to the total mass density ρ projected along a line of sight, where the *lensing sensitivity function*

$$g(z) = \frac{2D_L D_{LS}}{D_S} \quad (3)$$

reflects the efficiency of foreground gravitational lenses at different redshifts—containing a ratio of the angular diameter distance to a lens, the background source, and between the two. This can be more simply written as

$$\kappa \equiv \frac{1}{2}\left(\frac{\partial^2\Psi}{\partial x^2}+\frac{\partial^2\Psi}{\partial y^2}\right) \quad (4)$$

in terms of a 2D, projected version $\Psi(\boldsymbol{x})$ of the quasi-Newtonian gravitational potential. Two components of *shear*,

$$\{\gamma_1,\gamma_2\} \equiv \left\{\frac{1}{2}\left(\frac{\partial^2\Psi}{\partial x^2}-\frac{\partial^2\Psi}{\partial y^2}\right), \frac{\partial^2\Psi}{\partial x\partial y}\right\}, \quad (5)$$

describe stretches and compressions along (at 45° from) the x-axis.

The observed shapes of background galaxies can be described by a combination of their Gaussian-weighted quadrupole moments,

$$d \equiv \frac{\int\int I(\boldsymbol{x})W(\boldsymbol{x})r^2\,d^2\boldsymbol{x}}{\int\int I(\boldsymbol{x})W(\boldsymbol{x})\,d^2\boldsymbol{x}}, \quad (6)$$

$$\{\varepsilon_1,\varepsilon_2\} \equiv \frac{\int\int I(\boldsymbol{x})W(\boldsymbol{x})r^2[\cos(2\theta),\ \sin(2\theta)]\,d^2\boldsymbol{x}}{\int\int I(\boldsymbol{x})W(\boldsymbol{x})r^2\,d^2\boldsymbol{x}}, \quad (7)$$

where

$$W(\boldsymbol{x}) = e^{-r^2/2r_g^2}. \quad (8)$$

Although κ is generally the desired quantity, and could be obtained in principle from measurements of galaxy sizes (eq. [6])

TABLE 1
Survey Characteristics

Observation	Instrument	Primary Aperture (m)	Exposure Time (s)	Total Survey Time (hr)	Filter	Limiting AB Magnitude	Field of View (deg^2)	Pixel Scale (arcsec)	PSF (arcsec)
Ground	Subaru Suprime-Cam	8.2	5×360	5	i'	26.2	2.14	0.202	0.54
Space	*HST* ACS	2.4	4×507	863	F814W	26.6	1.67	0.03	0.12

or fluxes, this has proved difficult in practice, because expectations for these quantities prior to lensing are unknown. On the other hand, while galaxies have a natural dispersion of intrinsic ellipticities (eq. [7]), they are (almost) uncorrelated with each other in the absence of lensing, i.e., $\langle \varepsilon_i \rangle = 0$. Any correlation between the *observed* ellipticities of galaxies seen along adjacent lines of sight arises because their light has traversed similar intervening large-scale structure $\rho(\boldsymbol{x}, z)$. In practice, corrections to measured ellipticities also need to be made for the smearing of galaxies by the PSF, and for the differing susceptibilities of some galaxy morphologies to an input shear. For more details of this procedure, see, e.g., Kaiser et al. (1995, hereafter KSB95).

The observed shear can finally be transformed into convergence through their close relation in Fourier space,

$$\tilde{\kappa} = \frac{(l_1^2 - l_2)\tilde{\gamma}_1 + (2l_1 l_2)\tilde{\gamma}_2}{(l_1^2 + l_2^2)} \quad (9)$$

(Kaiser & Squires 1993). Furthermore, like any scalar quantity extracted from a vector field, a convergence signal can also be split into two independent components, $\kappa = \kappa^E + i\kappa^B$ (King & Schneider 2001). The grad-like "*E*-mode" is the signal produced by weak lensing. The curl-like "*B*-mode" is not produced by physical processes (except at very low levels, as described by Schneider et al. 2002), and therefore ought to be consistent with zero in the absence of systematics. Usefully, it contains the same noise properties as the *E*-mode signal—so it acts as an independent realization of noise in the field, and any significant deviations from zero alert one to the presence of residual systematics (such as imperfect correction for the PSF).

3. OBSERVATIONS AND DATA REDUCTION

3.1. *The COSMOS Data Sets*

Our data all cover the COSMOS survey field, a 1.64 deg^2 contiguous square, centered at R.A. = $10^{\rm h}00^{\rm m}28.6^{\rm s}$, decl. = $+02^\circ12'21.0''$ (J2000.0; Scoville et al. 2007a). The ground-based imaging was obtained in 11 mosaicked pointings of the Suprime-Cam camera at the prime focus of the Subaru telescope on Mauna Kea (Miyazaki et al. 2002b). These were taken on 2004 February 18 and 21, nights selected for their excellent observing conditions: the mean seeing was $0.54''$. The field constitutes part of a larger weak-lensing survey discussed, along with full details of the data quality and primary reduction pipeline, in Miyazaki et al. (2007) and A. Green et al. (in preparation). In fact, the relevant field in that survey covered a slightly larger area than the COSMOS field. The Subaru imaging was truncated when matching galaxy catalogs and was truncated *after* making convergence maps, to avoid edge effects associated with the Fourier transform operations in equation (9).

Our comparison is made possible by the unique availability of deep, panoramic space-based imaging of the COSMOS field (Scoville et al. 2007b). During *HST* cycles 13 and 14, 577 slightly overlapping pointings were obtained from *HST* ACS. Four dithered exposures at each pointing were stacked using the DRIZZLE algorithm (Fruchter & Hook 2002) to improve the native pixel scale of $0.05''$ and recover a final pixel scale of $0.03''$. Full details of the primary data reduction pipeline for the *HST* images are given in (Koekemoer et al. 2007).

It is important to emphasize that both the ACS and Suprime-Cam data exhibit idiosyncrasies that present significant challenges for weak-lensing analysis. For example, the atmospheric seeing varied during the two nights over which the Subaru data were obtained (see the first two nights in Fig. 1 of Miyazaki et al. 2007), and the distortions of the telescope's primary mirror under a gravity load were only passively corrected via a look-up table as it followed the field. In a future ground-based experiment, such as LSST or Pan-STARRS, seeing variations could be normalized over a survey by stacking a very large number of short, independent exposures taken over a long time period. Dome seeing could likewise be improved with future technologies. And while the telescope superstructure is particularly rigid at Subaru, active correction of the mirror support could undoubtedly improve future designs. Equivalently, the sky background seen from *HST* is affected by earthshine that depends on the telescope pointing (Leauthaud et al. 2007). The *HST* PSF also varies over time due to thermal fluctuations during each low-Earth orbit (Jee et al. 2007a; Rhodes et al. 2007). Finally, the charge transfer efficiency of the ACS CCD detectors had been significantly degraded by high-energy particles by the time the COSMOS data were obtained, and worsened during the observing window (Rhodes et al. 2007). The weak-lensing analysis of existing space-based data is compromised by the extent to which such hardware variations can be modeled. However, none of these problems are inherent to all space-based observations: future missions might eliminate all three effects by adopting a regular observing pattern, orbiting the Lagrange point L2, using radiation-hardened CCDs or a different detector technology altogether.

The relevant characteristics of the two data sets are summarized in Table 1, including limiting depths for a point source at 5 σ, in a $3''$ aperture from the ground and a $0.15''$ aperture from space (Capak et al. 2007). In addition to these images, the COSMOS field has been observed across all wavelengths from radio to X-rays. Of particular relevance here are (1) deep X-ray observations by *XMM* (Hasinger et al. 2007), which can be used to locate massive structures via thermal emission from hot gas; and (2) multicolor optical and near-IR imaging campaigns from the Subaru, Canada-France-Hawaii, Cerro Tololo, and Kitt Peak telescopes, which provide 15 additional bands and photometric redshifts (Capak et al. 2007; Mobasher et al. 2007). The photometric redshift estimation code uses Bayesian priors based on an adopted luminosity function, and includes reddening based on both Galactic and Calzetti extinction laws. The results were calibrated using 868 galaxies in the field brighter than $i' = 24$ and with spectroscopic redshifts. For galaxies closer than $z = 1.2$, the rms scatter in $(z_{\rm phot} - z_{\rm spec})/(1 + z_{\rm spec})$ is 0.031.

3.2. *Object Detection*

Objects were detected in the Subaru images using HFINDPEAKS from the Imcat package.[10] This finds the centroid and scale size r_g that maximizes the peak S/N of the image after smoothing with a Gaussian. The code also returns the half-light radius, r_h, of each galaxy. Galaxies were initially detected to magnitudes fainter than those for which it is possible to accurately measure shapes. To reduce noise in the final analysis, weights were given to each galaxy, and galaxies with a detection S/N < 14 were removed from the catalog altogether. The resulting surface density is $n_{\rm gal} = 42$ galaxies arcmin^{-2}.

Objects were detected in the ACS images using SExtractor (Bertin & Arnouts 1996) in a dual hot/cold configuration (Leauthaud et al. 2007), designed to identify both large and small objects while avoiding fragmentation of the former, or merging of the latter. The SExtractor centroids were then improved, and the best-fitting scale size was selected, via an iterative process during shape measurement. Galaxies smaller than $d = 0.11$ arcsec^2 or fainter than S/N ≈ 20 were removed from the catalog, and a weighting scheme was applied to faint galaxies as a function of their detection S/N (Leauthaud et al. 2007). Note that an absolute calibration of the S/N was difficult to determine in practice, because flux in adjacent pixels becomes correlated during DRIZZLE. The S/N cut corresponds approximately to a limiting magnitude F814W(AB) < 26.5 for a point source. The resulting surface density is $n_{\rm gal} = 71$ galaxies arcmin^{-2}, with a median redshift $z_{\rm med} = 1.2$.

3.3. *Shear Measurement*

Because the image characteristics of the two data sets are quite different, we adopted separate methods to measure galaxy shapes, remove PSF effects, and ultimately obtain the weak-lensing shear signal. Each of these methods has been optimized for the respective data sets, so our comparison will necessarily incorporate the limitations of each pipeline. We believe this is in the spirit of a fair comparison of ground versus space. To minimize any differences arising entirely from the algorithms themselves, however, we have intentionally adopted related methods from the same generation of software development and codes that have been well tested. Although newer shear measurement methods (Kaiser 2000; Bridle et al. 2001; Dahle et al. 2002; Refregier & Bacon 2003; Bernstein & Jarvis 2002; Hirata & Seljak 2003; Kuijken 2006; Massey et al. 2007a; Nakajima & Bernstein 2007) may offer improved performance, none has yet been sufficiently tested across both observing regimes.

The Subaru images were analyzed with the Hamana et al. (2003) implementation of the widely used KSB95 shear-measurement method. This particular implementation is a derivative of the "LV" pipeline tested in STEP (Heymans et al. 2005a; Massey et al. 2007d).

The *HST* images were analyzed with the Rhodes et al. (2000, hereafter RRG00) shear-measurement method. This is a perturbation of the KSB95 method for space-based data. It calculates the same quadrupole moments, but corrects them individually for the effects of convolution with the PSF, and only in the final stage takes the ratio 7. This is necessary because the small and cuspy diffraction-limited PSFs otherwise introduce divisions by very small (and noisy) numbers. The RRG00 method has been applied to *HST* WFPC2 (RRG00), STIS (Rhodes et al. 2004), and ACS data (Massey et al. 2007b). The ACS pipeline was thoroughly tested on simulated images during the creation of the COSMOS catalog (Leauthaud et al. 2007), and also for a continuation of STEP using simulated space-based images.

[10] Nick Kaiser's Imcat software package is available from http://www.ifa.hawaii.edu/~kaiser/imcat/.

4. STATISTICAL APPLICATIONS

4.1. *Shear-Shear Comparisons*

We now compare the global properties of our ground- and space-based shear catalogs, to determine the depth (and galaxy surface density) at which reliable shear measurement is possible from the ground. This will be relevant for many statistical applications, including measurements of the angular shear-shear correlation function that are typically used to constrain cosmological parameters. In such analyses, where statistical noise is reduced by averaging over many lines of sight, the key issue is the reliability and level of residual systematics in the shear measurement.

We assess the performance of the ground-based shear measurements against those from *the same galaxies* in space-based data, making the necessary but reasonable assumption that the shapes are much more reliable when measured from the much higher resolution images with a smaller PSF. Such a comparison is clearly only possible for the subset of galaxies contained in both catalogs. The two quantities of interest will be linearity in the comparison (the slope of the shear-shear comparison is equivalent to the STEP "calibration bias" parameter m) and the scatter (which represents the combined shear measurement noise from both *HST* and Subaru, plus any systematic effects).

We match galaxies whose positions agree to within $1''$, and produce a common catalog containing $n_{\rm gal} = 32$ galaxies arcmin^{-2}. Many objects in the Subaru galaxy catalog without matched counterparts in *HST* galaxy catalog have half-light radii on the limits of seeing and are likely to have been revealed as stars by the higher resolution data; in any case, the omitted objects had below-average weights in the Subaru catalog. The remaining unmatched objects are a combination of noisy/skewed galaxies with offset centroids, or galaxies that lie in regions of the *HST* images masked because of scattered light from nearby bright stars. For the following tests, we ignore the weights on remaining galaxies, and treat all objects equally.

Figure 1 shows a comparison of the shear estimators from our two catalogs. Since these include significant components of intrinsic ellipticity for each galaxy, we include only the matched subset of galaxies. Even so, there will inevitably be a small amount of scatter, because of measurement noise, and because the weight functions (eq. [8]) used in the ground- and space-based analyses do not necessarily have the same size r_g. Fortunately, neither of these will introduce bias for shear estimators (eq. [7]) because the shear susceptibility of each galaxy is calculated using the appropriate weight function, and parity invariance of the universe ensures that the ellipticity of a galaxy's outer wings cannot be systematically offset from that of the inner core. Perfect shear measurement from both instruments would yield a best-fit slope of unity. Using a least-squares method that minimizes the *perpendicular* distance to the best-fit line (rather than vertical distance because errors are present in both axes), we measure the best-fit linear relationship to have a slope of 0.87, indicating that the shears have been relatively underestimated from the ground. Furthermore, there is a non-Gaussian distribution of outlying shear estimates that would render a cosmic shear analysis less stable. The measurement noise is $\sigma_\gamma = 0.16$ per component, perpendicular to the best-fit line (note that this does not include intrinsic source ellipticity variance because the same galaxies feature in both catalogs).

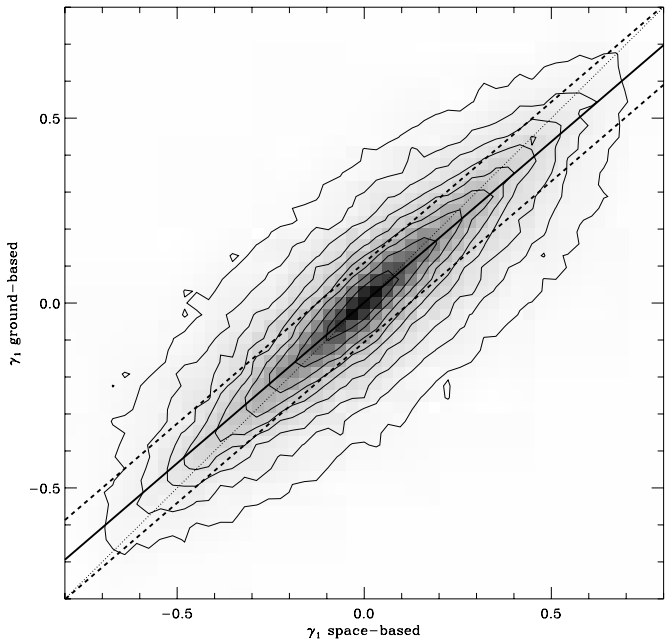

FIG. 1.—Comparison of shear estimators from galaxies seen in both Subaru and *HST* images. The gray scale shows the number of galaxies with different shear measurements. The outer contour includes 90% of the galaxies, and successive inner ones include 10% fewer. The solid line is the least-squares linear relation. Its slope of 0.87 indicates that shear estimators have been underestimated in the ground-based analysis, or that the catalog is still partially contaminated by stellar sources. This value is insensitive within 0.01 to the reintroduction of galaxy weights. Furthermore, the non-Gaussian wings of the scatter extend well beyond the rms error of 0.16, shown as dashed lines.

In Figure 2 we also test whether the measured calibration bias is affected by first binning galaxies in $1.4' \times 1.4'$ cells on the sky. Averaging the individual shear estimators lessens the influence of differently sized weight functions and reduces measurement noise and the effect of intrinsic ellipticities, producing an ensemble shear estimator more correlated with the true shear signal. The calibration bias remains unchanged regardless of the matched subset of galaxies that are used, justifying our galaxy-by-galaxy approach in Figure 1. Indeed, averaging multiple shear estimators can only remove information from a galaxy-by-galaxy analysis.

The overall performance in Figures 1 and 2 is a superposition of good shear estimators from bright and (in particular) large galaxies, plus smaller objects that cause most of the bias and scatter. Indeed, systematic errors could be completely eliminated by using only the very largest galaxies. However, the statistical noise in a cosmic shear analysis of shear-shear correlation functions scales as $\sigma_\gamma/(n_{\rm gal})^{1/2}$. An optimal strategy for any particular ground-based survey will involve catalog cuts requiring a tradeoff between systematic and statistical errors. However, the optimal cuts will vary as a function of survey area and depth. To produce a result of general interest, we therefore show in Figures 3 and 4 the resulting calibration bias, scatter, and galaxy density for a range of possible cuts in galaxy size and magnitude.

A simple result emerges from Figure 3. It is noticeable from the roughly horizontal and vertical contours that size and magnitude cuts seem to parameterize independent sources of error. Using existing shape-measurement methodology, shear can be measured from galaxies brighter than $i' = 24.5$ and larger than $r_h = 1.8$, with measurement noise $\sigma_\gamma \simeq 0.03$ and a calibration bias less than 3% (and only 1% with galaxy weighting), which is acceptable for competitive constraints from future surveys (Refregier et al. 2004; Amara & Refregier 2008).This leaves a surface density of $n_{\rm gal} = 15$ galaxies arcmin^2 from the ground, with a median redshift of $z_{\rm med} = 0.8$. The comparison with space-based data for these cuts is shown in Figure 5.

Note that we have not been able to test the reliability of space-based shear measurements using this method, nor even considered the population of small galaxies resolved only from space. Without data even better than ACS imaging to compare to, we resort to simulations. The full RRG00 pipeline was calibrated against simulated images by Leauthaud et al. (2007). However,

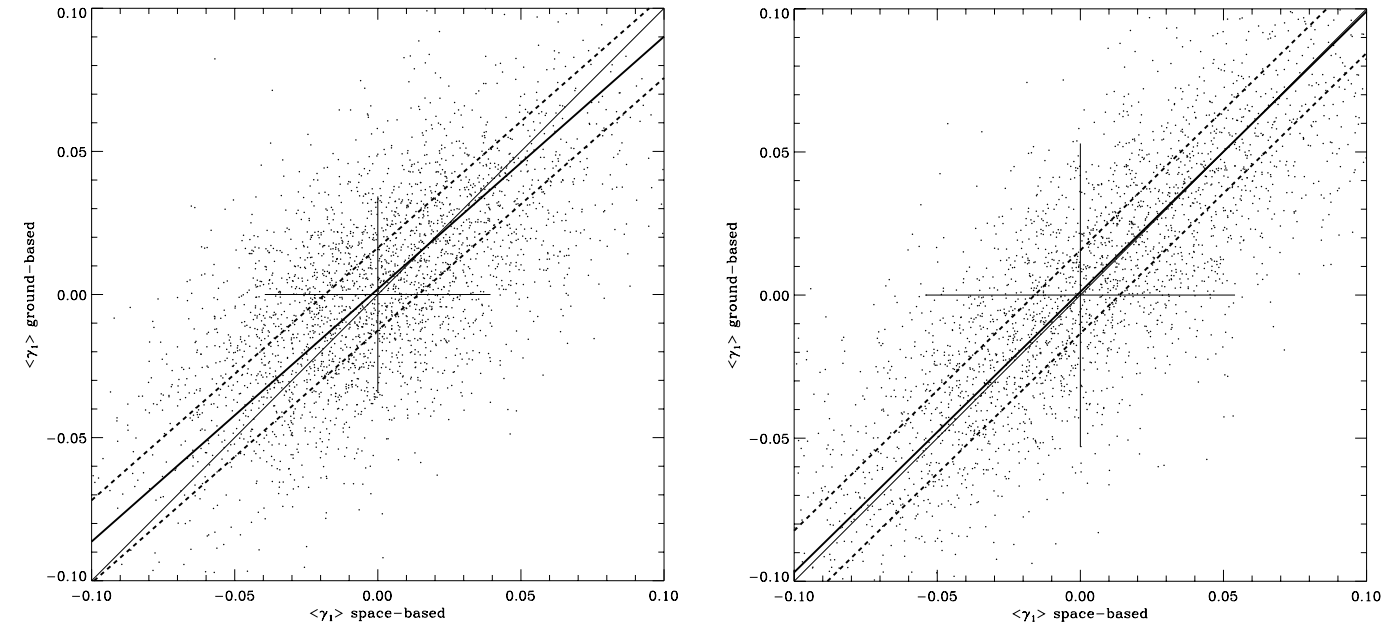

FIG. 2.—Comparison of shear estimators from Subaru and *HST* data, in square cells of 2 arcmin^2. In such a small region, the true shear signal is approximately constant, and should be traced by the mean of shear estimators from each galaxy. This analysis is parallel to that of Figs. 1 and 5, although scatter due to noise and measurements of ellipticity at different radii is reduced. The left panel shows the mean shear estimates derived from the full (matched) galaxy catalog, containing approximately 84 galaxies per data point. The cross at the origin shows the mean of the errors in each cell. The thick solid line shows the least-squares linear relation; its slope is 0.85. The right panel uses only galaxies brighter than $i' = 24.5$ and larger than $r_h = 1.8$. The error in each cell is now larger, because they contain only 29 galaxies on average. However, the least-squares linear slope is now 0.98.

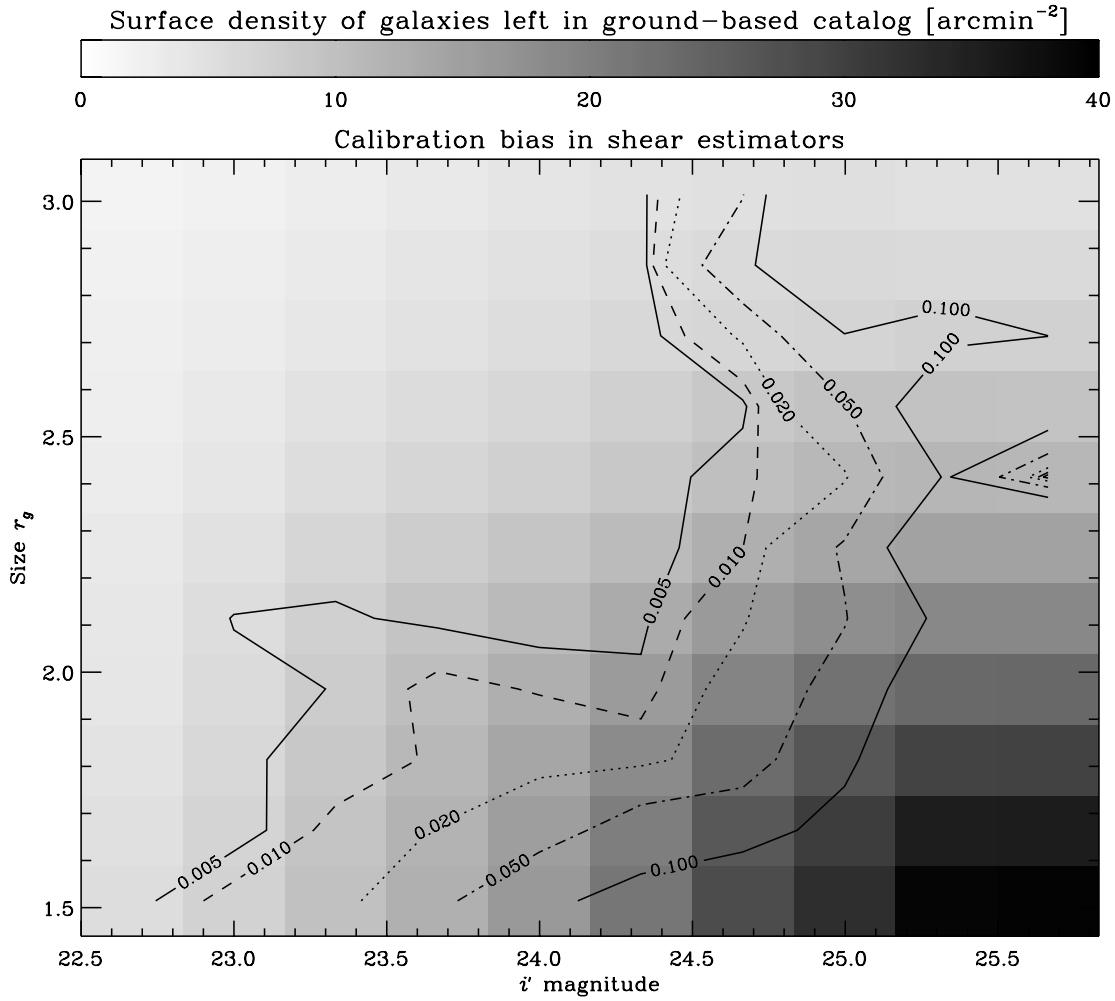

FIG. 3.—Relative calibration between shear estimators from galaxies in Subaru and *HST* data, for galaxies of different sizes and magnitudes. The contours show deviations from the ideal slope of unity in Fig. 1. For faint galaxies, these deviations tended to be an underestimation of shear in the Subaru pipeline relative to *HST*. There is some evidence that shears are overestimated in large, bright galaxies, although the small number of these objects means that the extrapolation is less certain. The calibration biases are calculated locally, for galaxies only in a given cell of (size, magnitude) space. On the other hand, the gray scale shows the cumulative number density of galaxies $n_{\rm gal}$ that would remain in a ground-based catalog, were cuts to be applied at the local values (i.e., including all larger and brighter galaxies).

of the 71 galaxies arcmin^{-2} in real ACS images, only the brightest 40 could be used by Massey et al. (2007b) to minimize the *B*-mode signal and overcome problems of CCD charge transfer inefficiency (CTI). This limitation clearly needs to be overcome, perhaps via a CTI correction algorithm like that developed for STIS by (Bristow 2004) and radiation-hardened detectors in future telescopes.

4.2. *Implications*

We now consider the implications of the results of our ground versus space shear comparisons in terms of the optimal approach for measuring shear for cosmological applications. Although we realize the étendue and imaging performance of future instruments can be expected to increase both on the ground and in space, we discuss the points arising from our *HST* and Subaru comparison in quite general terms.

An important criterion in survey applications is the useful data that can be obtained in a given amount of observing time; the *HST* and Subaru requirements for our comparison are summarized in Table 1. *HST* overheads approximately tripled the on-source exposure time, and, at Subaru, high-quality imaging can only be secured during periods of stable, high-quality seeing. These limitations arise from *HST*'s low Earth orbit and the fact that images with seeing worse than $\sim 0.8''$ are of little use for weak-lensing analysis (Bacon et al. 2001). Thus, the limitations from space are avoidable given the proper orbit for future weak-lensing missions but the ground-based limitations are more fundamental and challenging to overcome. Therefore, when coupled with other issues of observational visibility, it seems reasonable to incorporate a similar factor of inefficiency for a generic ground-based survey. Future surveys such as Pan-STARRS and LSST, which plan to co-add many short exposures with independent PSFs, may achieve near-uniform image quality by rejecting a certain fraction of exposures. But the relevant figure of merit will still be the fraction of time spent with seeing better than $0.8''$. Thus, the primary ground-based advantage in mapping speed can only arise from a superior field of view.

Subaru's significant advantage in survey speed compared to *HST* is mitigated by the higher angular resolution available from space. The substantial gain in surface density, a factor of 3–5, has two benefits. First, assuming that the additional (small) galaxies have a similar distribution of intrinsic ellipticities as the larger ones (cf. Massey et al. 2004; Leauthaud et al. 2007), and that the measurement noise on an average survey galaxy is constant (since

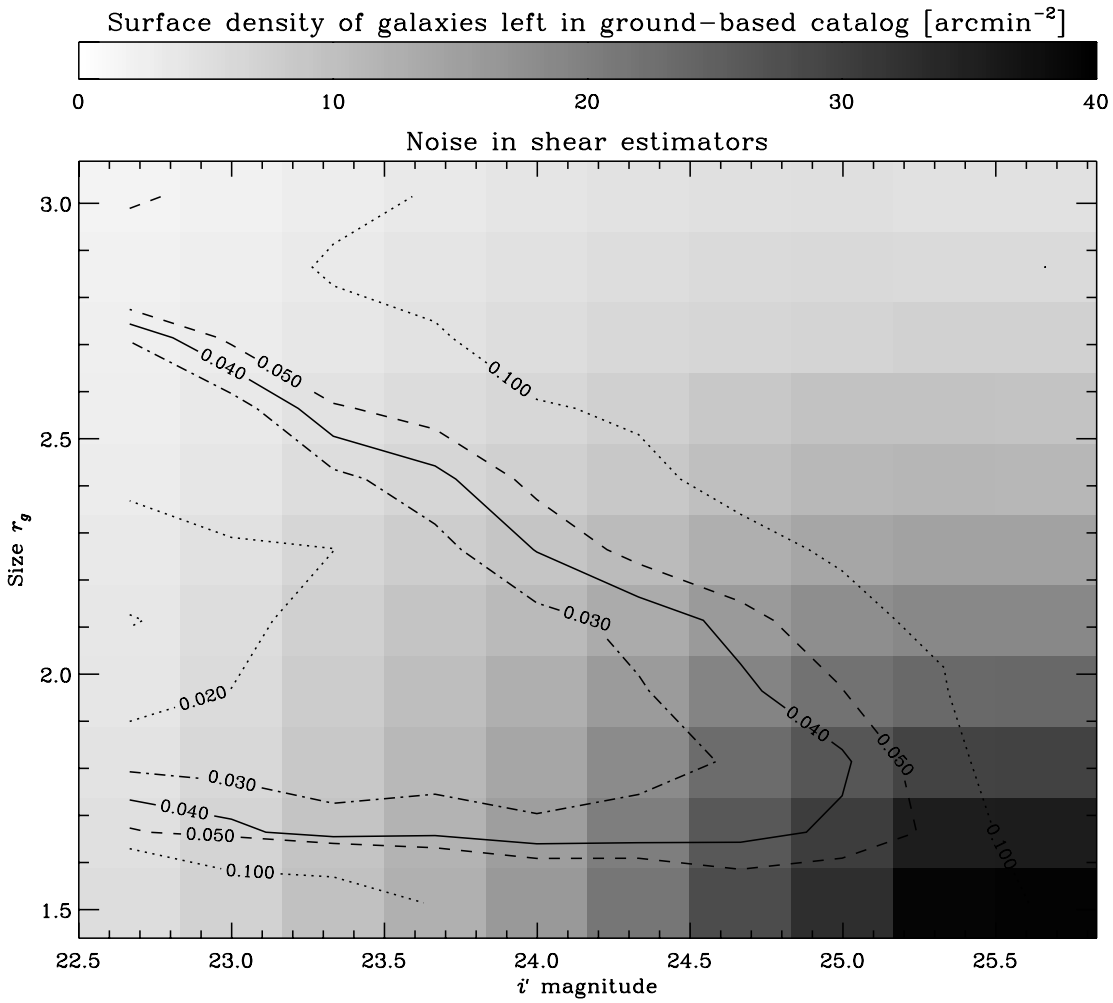

FIG. 4.—Combined noise in shear estimators from galaxies matched in catalogs from Subaru and *HST* data. The contours show σ_γ as a function of galaxy size and magnitude. As in Fig. 3, these are calculated only for galaxies with that particular size and magnitude. The contours close at the top merely because there are very few large, faint galaxies, so the rms scatter increases. The gray scale again shows the total number density of available galaxies.

their size distribution relative to the PSF is roughly independent of the PSF size), the mapping speed of *usable galaxies* becomes almost comparable. Second, *HST* achieves an increased density of galaxies at higher redshifts. Distant galaxies are more sensitive to the presence of low-redshift lenses. The shear signal grows proportionally to the median source redshift as $z_{\rm med}^{0.6} - z_{\rm med}^{0.8}$ (Jain & Seljak 1997). With the redshift distributions for galaxies shown in Figure 6, the total gain in signal-to-noise ratio for a 2D weak-lensing survey conducted from Subaru is further reduced.

The increased redshift range of the resolved galaxies in a space-based survey (Fig. 6) has several advantages for cosmological applications. This better enables their stratification into redshift bins for tomographic (3D) analyses. Tomographic techniques can tighten the constraints on cosmological parameters Ω_M and σ_8 by a factor of >3 (Massey et al. 2007b). A further advantage of deeper data includes the elimination of unwanted signal from the intrinsically correlated shapes of adjacent galaxies (King & Schneider 2003; Heymans & Heavens 2003).

Clearly, the above comparison is only quantitatively of value to present instruments. However, the main point to make is that an apparent 20–30 fold advantage of mapping speed of Subaru over *HST*, arising from its panoramic field of view, is readily eroded to a factor of $\simeq$2 for statistical applications if the lower surface density of resolved galaxies is taken into account. This advantage is further eroded for tomographic techniques where redshift reach is paramount. As both ground- and space-based instruments of the future will exploit wider fields and more stable PSFs, this gain for a space-based platform seems likely to remain for the most demanding applications.

5. MASS MAPS AND HALO DETECTION

We now investigate the reconstruction of maps of the mass distribution (Figs. 7 and 8), and the detection of individual mass peaks. The mass and redshift distribution $N(M, z)$ of several thousand lensing-selected clusters could be used to constrain cosmological models (Hamana et al. 2003; Wang et al. 2004; A. Green et al., in preparation). In addition, the physical properties of the dark matter particles can be investigated by comparing the detailed distribution of dark matter with that of baryons (Clowe et al. 2006b; Jee et al. 2007b). The key issues will be the angular resolution of reconstructed mass maps, as well as the mass and redshift range in which halos can be successfully detected. We treat this as an independent experiment from the previous section, beginning the comparison of ground- and space-based data afresh. In particular, we do *not* cut the Subaru data to the shallower depth discussed in § 4.1, to eliminate the last few systematic biases. The intent is not to align our two comparisons but rather to optimize each analysis as an independent experiment—as

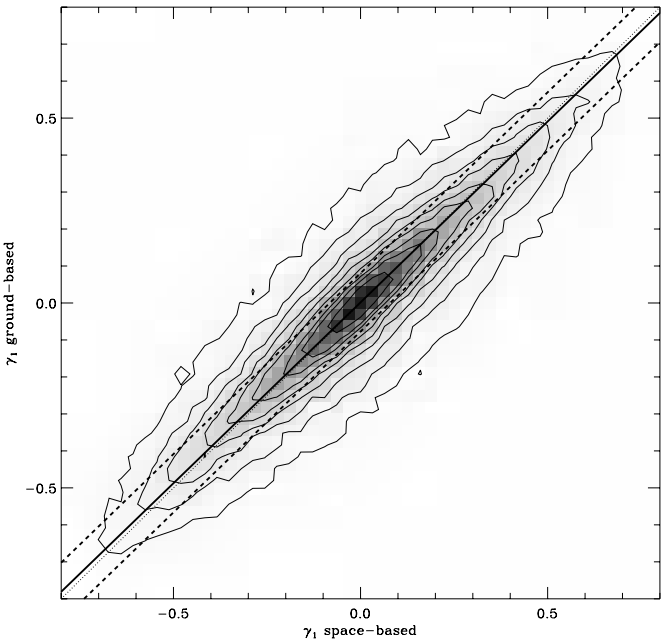

FIG. 5.—Same as Fig. 1, but for the subset of galaxies brighter than $i' = 24.5$ and larger than $r_h = 1.8''$. The total least-squares slope is 0.97, implying an almost unbiased recovery of the shear signal from Subaru, and the data is better and more symmetrically enclosed within the rms scatter of 0.11.

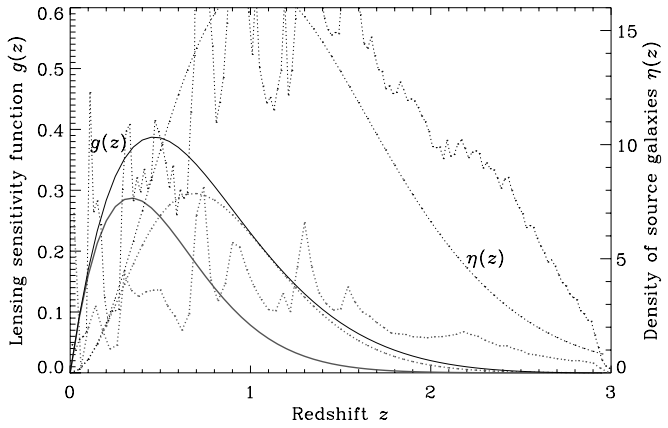

FIG. 6.—Dotted lines show the redshift distribution of source galaxies from *HST* (*black*) and Subaru (*gray*) imaging surveys, for the catalog cuts used in Fig. 5. The jagged lines show the measured photo-z values, and the smooth curves assume a simple parametric form for the background galaxy redshift distribution from Smail et al. (1994), with $\alpha = 2$, $\beta = 1.5$, $z_{\rm med} = 0.8$ or 1.2, and an overall normalization to reproduce the observed number density of galaxies. The solid lines show the corresponding lensing sensitivity functions calculated from the analytic curves. These lie always in front of the source galaxies but are notably higher for a space-based survey, particularly at redshifts greater than 0.5. [*See the electronic edition of the Journal for a color version of this figure.*]

would be the case if either were being undertaken as self-contained observations.

Unfortunately, even with the unprecedented investment of *HST* time for the COSMOS survey, we can expect the number of lensing-detected structures in this finite field to be modest. At the Subaru depth, a surface density of $\sim$5 halos deg^{-2} (Miyazaki et al. 2007) implies that only around eight halos are likely to be found in the COSMOS field. Thus, we recognize in this comparison that the statistical significance of our results will be quite limited.

5.1. *Residual Systematics*

First, we consider the *B*-mode signal. As discussed in § 2, the *B*-modes act as an independent realization of noise in the mass map, and locally highlight any problems with the correction for PSF or other effects peculiar to the (two very different) instruments. Unsurprisingly, a visual inspection of Figure 8 shows that the *B*-mode signal is significantly lower in our space-based data, with fewer *B*-mode peaks. The overall noise level is reduced, and holes arising from masked foreground stars are also smaller and less frequent. In the ground-based maps, these create additional edges that lead to spurious effects during the Fourier transforms required by equation (9). The extended gaps are caused by difficulties modeling the PSF near the edge of the field of view, and could be eliminated in future surveys by more conservative tiling strategies.

The southwest corner of the field has been troublesome throughout our analysis. This pointing was observed in slightly worse seeing, so the density of galaxies is reduced and the noise in the mass reconstruction is higher.

5.2. *Halo Detection*

The higher surface density of background galaxies from space also improves the reconstruction of the *E*-mode "mass map" convergence field. The noise is lower and the angular resolution higher (although to aid comparison, both panels in Fig. 7 are smoothed to the same scale). Several of the key features are qualitatively similar, but we are struck by the significant differences in the prominence of other mass peaks. To evaluate the robustness of detections, we employ an automated peak-finding algorithm.

Following Miyazaki et al. (2007), we smooth the convergence maps by a Gaussian kernel of rms width $1'$ and find local maxima with detection significance $\nu > 4$ (assuming Gaussian errors on the shear measured within $0.7'$ cells on the sky equal to the dispersion of those galaxy shears). Five peaks (marked A, B, C, D, and K in Fig. 7) are then identified in the ground-based data. However, two of these are near boundaries of the field mask. Imposing the rigorous restrictions discussed by Miyazaki et al. (2007), we find that only peaks A, B, and C remain (cf. Table 3 in Miyazaki et al. 2007). All three are also detected in a space-based lensing analysis, the 3D distribution of galaxies, and as extended sources in X-ray data (Hasinger et al. 2007; Finoguenov et al. 2007). Assuming the mass-luminosity relation adopted by Finoguenov et al. (2007), the detection threshold of this very deep X-ray data is well below that expected for lensing up to redshift $\sim$1, so this acts as an ideal external arbiter (of course, X-ray mass-observable relations are somewhat uncertain). The properties of the three clusters are summarized in Table 2 and demonstrate excellent agreement between the ground- and space-based data using the formalism of Miyazaki et al. (2007).

Cluster A (SJ J0959.6+0231) is the most massive structure inside the COSMOS field, easily detected at many wavelengths. It appears to be in the process of a major merger, and has been studied individually by Guzzo et al. (2007), who also obtained a spectroscopic redshift of $z = 0.73$. Cluster B (SL J1001.4+0159) is associated with an X-ray peak and overdensity of galaxies at $z_{\rm phot} = 0.35$. There is a second set of galaxies at $z_{\rm phot} = 0.85$ within $2'$, which undoubtedly complicates the interpretation a little, but our results are consistent with this high-redshift projection being a minor perturbation. Cluster C (NSC J100047+013912) is yet more local ($z = 0.22$; Miyazaki et al. 2007) and appears large on the sky. Only part of this cluster is inside the

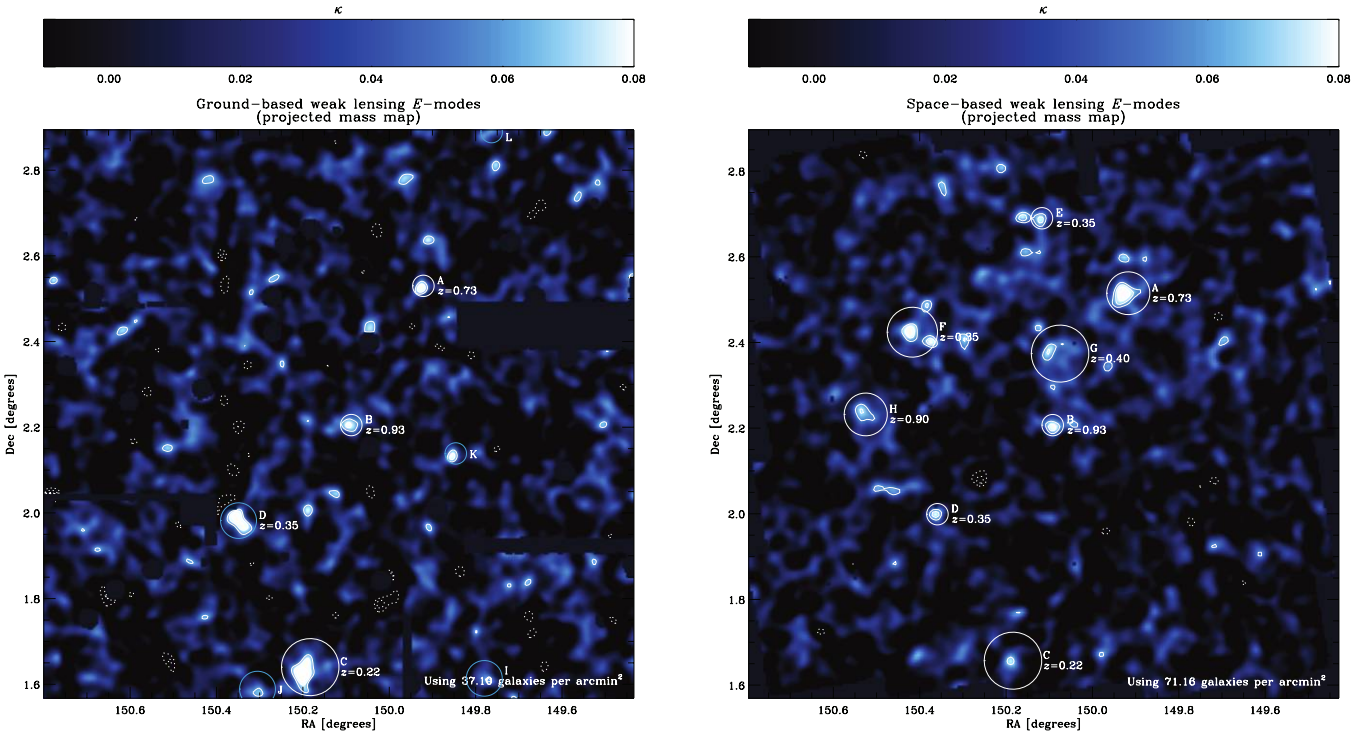

FIG. 7.—Convergence *E*-mode maps from Subaru (*left*) and *HST* (*right*), after smoothing by a 1′ Gaussian kernel. The data presented in the left panel are identical to that in Fig. 13 of Miyazaki et al. (2007), except that the field has been slightly truncated to match the right panel. Convergence is proportional to the total projected mass along a line of sight, modulated by the lensing sensitivity function (eq. [3]) plotted in Fig. 6. Contours are drawn at detection significances of 3, 4, and 5 σ, with dashed lines for underdensities. Clusters A, B, C, and D are detected in both maps. Other peaks E–L are only detected in one of the two. White enclosing circles denote clusters deemed "secure" by the rigorous standards of Miyazaki et al. (2007), and cyan circles denote "unsecure" clusters. The size of the circles shows the size of the smoothing kernel that maximizes detection significance, enlarged by a factor of 2 for clarity.

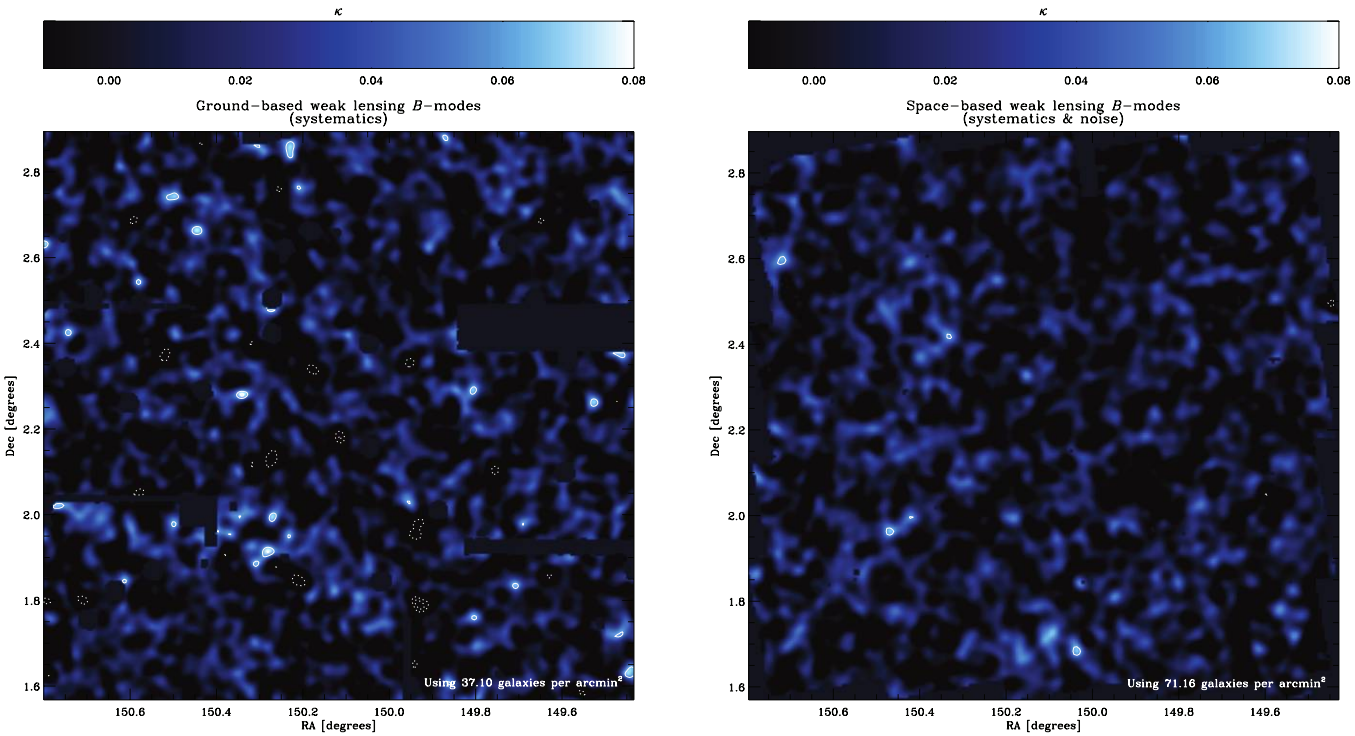

FIG. 8.—Convergence *B*-mode maps from Subaru (*left*) and *HST* (*right*) data. These are not produced by physical gravitational lensing, so deviations from zero include a combination of spurious effects from, e.g., imperfect PSF correction, plus a realization of statistical noise. We note that the circular holes are due to masking of foreground stars and the extended gaps are due to difficulty in modeling the PSF on the edges of each pointing. The smoothing scales, color ramps, and contours are identical to those in Fig. 7.

TABLE 2
CLUSTER MASSES

Cluster	R.A.	Decl.	Redshift	*XMM* Mass ($10^{14}\ M_\odot$)	*HST* Mass ($10^{14}\ M_\odot$)	Subaru Mass ($10^{14}\ M_\odot$)
A	149.917	2.515	0.73	1.90 ± 0.05	23^{+13}_{-8}	13^{+33}_{-9}
B	150.359	1.999	0.35	0.10 ± 0.01	9^{+7}_{-4}	17^{+13}_{-7}
C	150.184	1.657	0.22	1.01 ± 0.02	17^{+17}_{-9}	55^{+55}_{-27}

NOTE.—Units of right ascension are hours, minutes, and seconds, and units of declination are degrees, arcminutes, and arcseconds.

region of *HST* imaging, so the space-based signal is significantly weakened, and the mass is potentially underestimated by *HST*.

To broaden our search, and test the limits of detectability, we additionally investigate the multiscale procedure of Hamana et al. (2003). For this, we smooth the convergence maps with Gaussian filters of rms width between $0.5'$ and $4'$, identifying local maxima inside the mask on each scale. For each peak with a detection signal-to-noise ratio $\nu > 4$ on any scale, we record ν and the smoothing scale that maximizes ν. We also drop the restrictions on distance from the mask boundaries. This will increase the number of detected peaks, but at the expense of potentially introducing some spurious features. We then search for counterparts in the other data set, within $3'$ of detected peaks.

With the above criteria, we identify four mass peaks common to both convergence maps (A, B, C, and D). Cluster D is within $3'$ of an X-ray peak, and an overdensity of galaxies at photometric redshifts $z_{\rm phot} = 0.93$. This redshift is rather high for a lensing analysis, and it was flagged as "unsecure" by Miyazaki et al. (2007) because it is near a boundary in the image mask. However, the tentative Subaru detection is strengthened by the confirmation from *HST*, and appears to be robust.

Peaks E, F, G, and H (also marked on Fig. 7) are seen only in the space-based map. The first three correspond to extended X-ray emission from clusters with masses M_{500} in the range $(2-4) \times 10^{13}\ M_\odot$ (Finoguenov et al. 2007). Peak H is more massive ($M_{500} = 1.8 \times 10^{14}\ M_\odot$), but is at very high redshift ($z = 0.90$). All four of these peaks are real detections; however, no counterparts within $3'$ are seen in the ground-based map, even down to $\nu > 3$. Most likely, this is because of their lower mass and higher redshift (Hamana et al. 2003). The detection of peak G was prevented in the ground-based data by a bright foreground star.

Conversely, peaks I, J, K, and L are detected only in the ground-based map. Peaks I and J are real, but lie just outside the *HST* imaging. There is an extended X-ray source at peak I, with unknown redshift, and a projection of two $M_{500} \approx 2 \times 10^{13}\ M_\odot$ clusters at redshifts $z = 0.40$ and 0.75 at peak J (Finoguenov et al. 2007). In both cases, there is a weak $\nu < 3$ signal in the *HST* data, from the wings of the cluster. Peak K was detected in the Miyazaki et al. (2007) analysis, but again flagged as "unsecure" because it is near the edge of a pointing. It does align with a slight, $\nu < 3$ detection in the space-based map, but there is no X-ray counterpart. This may be a spurious peak with chance coincidence, or perhaps a very distant object. Peak L appears to be spurious: such noise artifacts are more common near the edge of the field.

In summary, to the extent that we can draw conclusions from such a small sample, there is very good agreement between the primary halo catalog drawn from the ground-based data and that independently found from the space-based data. Additional halos of lower mass and higher redshift are seen in the space-based catalog, and those located uniquely in the ground-based data can be understood in the context of either being outside the space-based region or close to its periphery.

5.3. *Halo Mass Estimation*

We now attempt to measure the total mass of each of the three halos (A–C) securely detected from both the ground and space. We assume that the clusters have an NFW density profile

$$\rho(r) = \delta_c \rho_c / (r/r_s)(1 + r/r_s)^2 \qquad (10)$$

(Navarro et al. 1996), where δ_c is a function of the cluster's concentration c and scale size $r_s \equiv r_{200}/c$, and r_{200} is the radius within which the mean density is 200 times the critical density.

The shear profile of an NFW cluster is derived by King & Schneider (2001). We perform a maximum likelihood fit to the log (mass) and concentration parameters, using the shear measurements from all galaxies within $10'$ of the peak convergence signal, averaged in radial bins of $0.5'$.

It has been variously noted (J. Bergé & S. Paulin-Henrikkson, private communication) that fitting noisy data of individual clusters with an NFW profile does permit large (and therefore massive) models with unnaturally low concentration values. To counter this effect, we impose a concentration prior, using the lognormal distribution found for all halos in the Millenium Simulation as a function of mass by Neto et al. (2007, eqs. [5] and [6] and Fig. 6). The resulting likelihood surfaces are shown in Figure 9, with the effect of the prior being to close the bottom of the contours. Table 2 lists the best-fit masses and 68% confidence limits after marginalizing over concentration in the range $1 < c < 10$.

Although our common sample is small, there is an encouraging agreement between the detailed properties of the clusters recovered from the ground and from space. For the higher redshift cluster A, our space-based data do put significantly tighter constraints on the mass and concentration than our ground-based data. However, for the lower redshift clusters B and C, the results are satisfyingly similar. We note again that cluster C is partially outside the *HST* imaging. Since shears are only measured around one half of the cluster, the statistical errors in the space-based analysis are larger and its mass could be underestimated. Certainly, for massive clusters with redshifts $0.2 \lesssim z \lesssim 0.5$, it appears that our ground-based depth and resolution is adequate. The main benefit of space-based imaging is in the measurement of lower mass halos and higher redshift clusters, plus the increased resolution to further investigate the distribution of their masses.

6. DISCUSSION

We have performed independent weak-lensing analyses of Subaru and *Hubble Space Telescope* (*HST*) imaging data in the COSMOS field. Our comparisons of the observed shear and convergence signals complement independent approaches based on

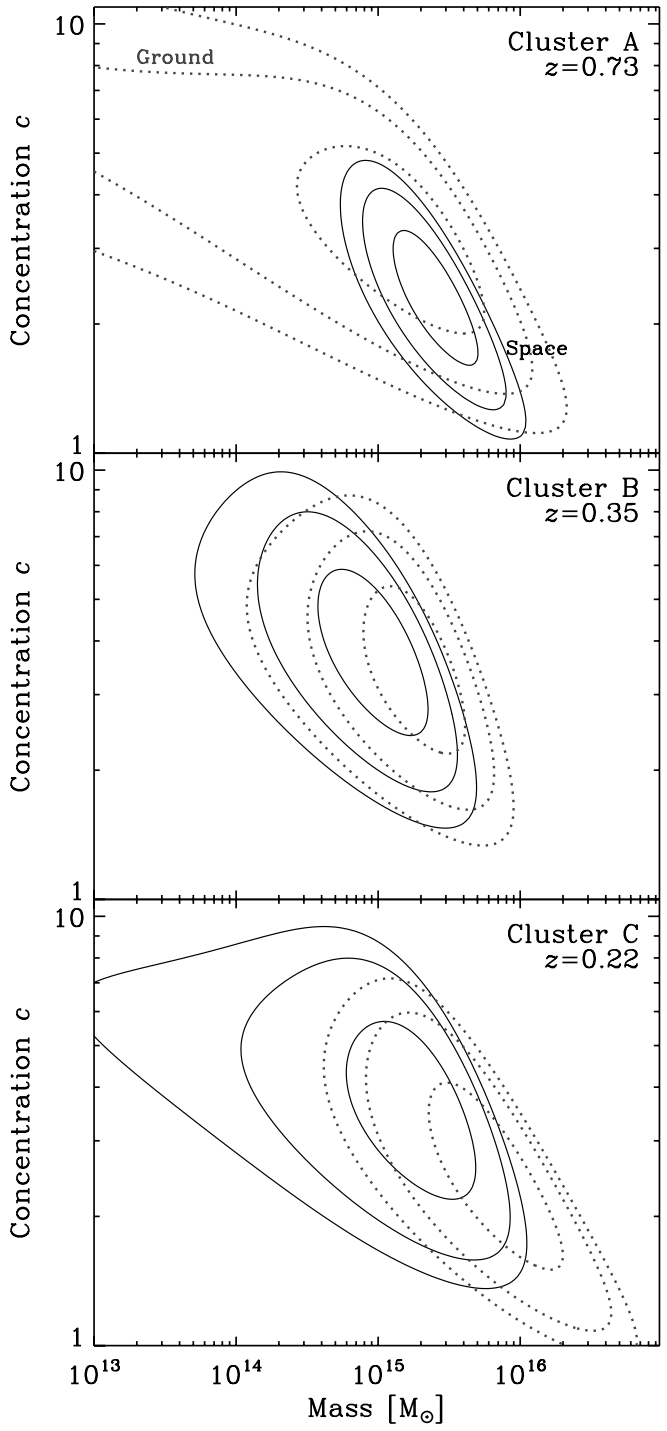

FIG. 9.—Best-fit mass and concentration index of three clusters in the COSMOS field, assuming NFW radial mass profiles. The contours show the 68%, 95%, and 99% confidence regions obtained from Subaru (*dotted lines*) and *HST* (*solid lines*) data. [*See the electronic edition of the Journal for a color version of this figure*.]

blind analyses of idealized simulated data (Heymans et al. 2005a; Massey et al. 2007d).

For statistical "cosmic shear" analyses, shear measurement with the Subaru telescope can, using existing measurement techniques, achieve a bias of less than 1% relative to higher resolution space-based data, but only for galaxies with large angular sizes corresponding to a reduced galaxy surface density of 15 arcmin^{-2}. One limitation of our approach is that we have no way to verify the validity of our analysis of the additional, smaller galaxies uniquely probed in the *HST* data.

Although a factor of $\sim$3 shortfall in surface density may seem inconsequential given the lower cost and improved areal mapping speed of Suprime-Cam versus ACS, accompanying this limitation is a reduction in survey depth and hence the redshift distribution of background sources. More distant sources offer a larger signal for a given gravitational lens. Moreover, the more limited redshift range implied for the lensing dark matter also reduces the utility of tomographical tests (Bacon et al. 2005; Massey et al. 2007b) that offer great promise for cosmological parameter constraints.

While it is clearly dangerous to generalize our conclusions to imply restrictions on the capabilities of all future ground-based cameras, we note that even with an 8 m aperture, our Subaru data are shallower, in terms of usable galaxies, than even a modest exposure undertaken with *HST*. Increased exposure times can be implemented as easily from space as from the ground. However, it is unclear whether increased ground-based exposure times would circumvent the ground-based floor, because the smallest galaxies simply cannot be resolved; a question not considered explicitly in this analysis but worthy of investigation. One previous analysis (Bacon et al. 2001) suggested that $R \sim 25.2$ data collected in seeing worse than $0.8''$ are of little use. The relevant quantities for a large-scale survey making statistical measurements are thus the time-averaged seeing and the fraction of time for which the seeing is better than that needed to resolve its faintest galaxies.

More generally, weak-lensing measurements from the ground will be affected by *variable* atmospheric seeing. Surveys such as PanSTARRS and LSST propose a strategy of co-adding many shorter exposures. Stacked images should achieve a near-uniform image quality by virtue of the independent PSFs applying to each short exposure. The final data can then be selected according to the required image quality by rejecting a certain fraction of exposures. Variable seeing is of particular concern for the reconstruction of mass maps (cf. A. Green et al., in preparation). Difficulties in the analysis of one pointing in the southwest corner of the Subaru map resulted in a patchy recovery of large-scale structure, with more noise and a lower range of probed redshift in certain regions.

Concerning the mapping of structure, it is reassuring that the four most massive clusters out of eight detected with *HST* are detected at >4 σ by Subaru—with one intriguing additional candidate and two further examples located by Subaru just outside the *HST* field of view. Reassuringly, the three clusters conservatively deemed "secure" by the independent analysis of Miyazaki et al. (2007) have each been confirmed via *HST* weak lensing and X-ray observations. The physical properties (masses and radial profiles) of the four massive halos in common are remarkably consistent in both data sets.

Our two main conclusions from this comparison are therefore:

1. For a given exposure time, the surface density of galaxies whose shapes can be reliably measured is considerably lower with Subaru than *HST*. This has significant implications in both the mapping speed for an effective weak-lensing survey, as well as the implied depth over which tomographic or 3D analyses can be undertaken. As 3D techniques will tighten constraints on cosmological parameters by factors of >3, this is an important point, particularly in probing dark energy via measures of the growth of structure and the redshift-distance relation. As an aside to this study we also note that the most complete implementation of 3D lensing will almost certainly require deep near-IR imaging

from space to provide sufficiently accurate photometric redshifts of the faintest galaxies.

2. With present technology and data analysis methods, a state-of-the-art ground-based camera such as Suprime-Cam on a large-aperture telescope such as the 8 m Subaru is capable of reliably locating halos whose masses extend down to a few 10^{14} $M_{\odot}$ over panoramic fields. Although our sample is small, we find no biases in our ground-based results at this mass level. The increased surface density of galaxies resolved from space does yield improved maps of the mass distribution. As shown in Figures 7 and 8, both the statistical noise and the systematic contamination in the *B*-mode are significantly reduced. The improved spatial resolution of mass reconstructions from *HST* clearly enables the detection of lower mass halos, as well as structures over a wider range of redshifts (see Massey et al. 2007c).

Overall, therefore, it appears that a large-aperture telescope equipped with a panoramic camera can perform several weak-lensing programs remarkably well. Our tests of Subaru's peformance compared to *HST* readily justify a new generation of dedicated ground-based imaging surveys. Two dimensional statistical analyses will be able to produce order-of-magnitude improvements in weak-lensing constraints, using proven hardware technology with existing software pipelines. On the other hand, a wide-field space-based imager offers a much increased surface density of usable galaxies and a concomitant increase in the depth over which lensing structures are being mapped in three dimensions. The additional benefit of a stable PSF for a future space-based platform will offer a yet further advantage via the control of systematical effects that clearly plague current analyses.

This work is supported by the US Department of Energy under contract DE-FG02-04ER41316. J. R.'s contribution was carried out at the Jet Propulsion Laboratory, California Institute of Technology, under a contract with the National Aeronautics and Space Administration and funded through the internal Research and Technology Development program. The analysis is based on observations with the NASA/ESA *Hubble Space Telescope*, obtained at the Space Telescope Science Institute, which is operated by Association of Universities for Research in Astronomy, Inc., under NASA contract NAS 5-26555. It is also based on data collected at the Subaru Telescope, operated by the National Astronomical Observatory of Japan. We acknowledge the careful comments of a referee and also valuable input from Zeljko Ivezik, Alexandre Refregier, James Taylor, and Alexis Finoguenov. We particularly thank Alexie Leauthaud and Takashi Hamana for help with the two galaxy catalogs. We also gratefully acknowledge the contributions of the entire COSMOS collaboration, consisting of more than 70 scientists worldwide. More information on the COSMOS survey is available from http://www.astro.caltech.edu/~cosmos.

REFERENCES

Amara, A., & Refregier, A. 2008, MNRAS, in press (astro-ph/0710.5171)
Bacon, D., Refregier, A., Clowe, D., & Ellis, R. 2001, MNRAS, 325, 1065
Bacon, D., Refregier, A., & Ellis, R. 2000, MNRAS, 318, 625
Bacon, D., et al. 2005, MNRAS, 363, 723
Bernstein, G., & Jarvis, M. 2002, AJ, 123, 583
Bertin, E., & Arnouts, S. 1996, A&AS, 117, 393
Bridle, S., Kneib, J.-P., Bardeau, S., & Gull, S. 2001, in The Shapes of Galaxies and Their Dark Matter Halos, ed. P. Natarajan (Singapore: World Scientific), 38
Bristow, P. 2004, in ASP Conf. Proc. 314, Astronomical Data Analysis Software and Systems XIII, ed. F. Ochsenbein, M. G. Allen, & D. Egret (San Francisco: ASP), 780
Brown, M., Taylor, A., Bacon, D., Gray, M., Dye, S., Meisenheimer, K., & Wolf, C. 2003, MNRAS, 341, 100
Capak, P., et al. 2007, ApJS, 172, 99
Clowe, D., et al. 2006b, ApJ, 648, L109
Dahle, H., Kaiser, N., Irgens, R., Lilje, P., & Maddox, S. 2002, ApJS, 139, 313
Finoguenov, A., et al. 2007, ApJS, 172, 182
Fruchter, A., & Hook, R. 2002, PASP, 114, 144
Guzzo, L., et al. 2007, ApJS, 172, 254
Hamana, T., et al. 2003, ApJ, 597, 98
Hasinger, G., et al. 2007, ApJS, 172, 29
Heymans, C., & Heavens, A. 2003, MNRAS, 339, 711
Heymans, C., et al. 2005a, MNRAS, 368, 1323
———. 2005b, MNRAS, 361, 160
Hirata, C., & Seljak, U. 2003, MNRAS, 343, 459
Hoekstra, H., et al. 2006, ApJ, 647, 116
Jain, B., & Seljak, U. 1997, ApJ, 484, 560
Jee, J., et al. 2007a, ApJ, 661, 728
———. 2007b, ApJ, 661, 728
Kaiser, N. 2000, ApJ, 537, 555
Kaiser, N., & Squires, G. 1993, ApJ, 404, 441
Kaiser, N., Squires, G., & Broadhurst, T, 1995, ApJ, 449, 460 (KSB95)
Kaiser, N., Wilson, G., & Luppino, G. 2000, ApJ, submitted (astro-ph/0003338)
King, L., & Schneider, P. 2001, A&A, 369, 1
———. 2003, A&A, 398, 23
Kitching, T., Heavens, A., Taylor, A., Brown, M., Meisenheimer, K., Wolf, C., Gray, M., & Bacon, D. 2007, MNRAS, 376, 771
Kneib, J.-P., et al. 2003, ApJ, 598, 804
Koekemoer, A., et al. 2007, ApJS, 172, 196
Kuijken, K. 2006, A&A, 456, 827
Lampton, M., Sholl, M., Jelinsky, P., & Stabenau, H. 2006, BAAS, 209, 980
Leauthaud, A., et al. 2007, ApJS, 172, 219
Massey, R., Rowe, B., Refregier, A., Bacon, D., & Bergé, J. 2007a, MNRAS, 380, 229
Massey, R., et al. 2004, AJ, 127, 3089
———. 2007b, ApJS, 172, 239
———. 2007c, Nature, 445, 286
———. 2007d, MNRAS, 376, 13
Mellier, Y. 1999, ARA&A, 37, 127
Miyazaki, S., et al. 2002a, ApJ, 580, L97
———. 2002b, PASJ, 54, 833
———. 2007, ApJ, 669, 714
Mobasher, B., et al. 2007, ApJS, 172, 117
Nakajima, R., & Bernstein, G. 2007, AJ, 133, 1763
Navarro, J., Frenk, C., & White, S. 1996, ApJ, 462, 563
Neto, A., et al. 2007, MNRAS, 381, 1450
Refregier, A. 2003, ARA&A, 41, 645
Refregier, A., & Bacon,D. 2003, MNRAS, 338, 48
Refregier, A., et al. 2004, AJ, 127, 3102
Rhodes, J., Refregier, A., & Groth, E. 2000, ApJ, 536, 79 (RRG00)
Rhodes, J., et al. 2004, ApJ, 605, 29
———. 2007, ApJS, 172, 203
Schirmer, M., et al. 2007, A&A, 462, 875
Schneider, P., Van Waerbeke, L., & Mellier, Y. 2002, A&A, 389, 729
Scoville, N., et al. 2007a, ApJS, 172, 1
———. 2007b, ApJS, 172, 38
Semboloni, E., et al. 2006, A&A, 452, 51
Smail, I., Ellis, R., & Fitchett, M. 1994, MNRAS, 270, 245
Taniguchi, Y., et al. 2007, ApJS, 172, 9
van Waerbeke, L., et al. 2000, A&A, 358, 30
Wang, S., et al. 2004, Phys. Rev. D., 70, 123008
Wittman, D., Dell'Antonio, I., Hughes, J., Margoniner, V., Tyson, J., Cohen, J., & Norman, D. 2006, ApJ, 643, 128
Wittman, D., et al. 2000, Nature, 405, 143
———. 2005, ApJ, 632, L5